Journal of Molecular Modeling (2021) 27: 365
https://doi.org/10.1007/s00894-021-04980-1

ORIGINAL PAPER

Theoretical investigation of substituent effects on the relative stabilities and electronic structure of $[B_nX_n]^{2-}$ clusters

Duygu Tahaoğlu[1] · Fahri Alkan[1] · Murat Durandurdu[1]

Received: 20 August 2021 / Accepted: 8 November 2021 / Published online: 29 November 2021

Abstract

In this study, we provide a theoretical evaluation of relative stabilities and electronic structure for $[B_nX_n]^{2-}$ clusters ($n = 10$, 12, 13, 14, 15, 16). Structural and electronic characteristics of $[B_nX_n]^{2-}$ clusters are examined by comparison with the $[B_{12}X_{12}]^{2-}$ counterparts with a focus on the substituent effects (X = H, F, Cl, Br, CN, BO, OH, NH_2) on the electronic structure, electron detachment energies, formation enthalpies, and charge distributions. For the electronic structure and electron detachment energies, substituent effects on boron clusters are shown to follow a very similar trend to the mesomeric and inductive effects (±M and ±I) of π-conjugated systems, and the most stable derivatives in terms of HOMO/LUMO and electron detachment energies are calculated for CN and BO substituents due to strong -M effects. In the case of formation enthalpies for larger boron clusters ($n \geq 13$), the icosahedral barrier is shown to increase with the halogen and CN substitution, whereas it is possible to reduce the icosahedral barrier for the cases of X = OH and NH_2. It is shown that this reduction results from destabilizing the $[B_{12}X_{12}]^{2-}$ cluster with electronic (+M) and symmetry effects induced by OH and NH_2 ligands.

Keywords Boron clusters · Icosahedral barrier · Mesomeric effect · Inductive effect · Substitution

Introduction

Boron has a rich and versatile coordination chemistry with an expectation of having analogous properties to carbon in respect of forming various bonds with different elements, but through different dynamics compared to carbon. As a result of its electron deficiency and strong bonding capacity with large coordination numbers via multicenter bonding, boron-containing systems have attracted considerable research interest in cluster chemistry [1–4]. For a few decades, the focus of the experimental and theoretical studies on various boron clusters such as bare boron clusters, boranes, carboranes, and metallaboranes [5–8] has been to identify stable and low-energy conformations while exploring their electronic and chemical properties for potential applications [9]. Many boranes and derivative clusters have been theoretically predicted and experimentally observed as stable gas phase dianions [10–15], which make them potential materials for the use in different applications as charged anion class. More recently, (car)boranes and their derivatives have shown to be promising candidates as electrolytes for energy storage applications [16–18]. Polyhedral (car)boranes are also good alternatives as closomers [19] for their applications ranging from materials science to medicine.

Among the investigated closo-borane clusters, icosahedral $[B_{12}H_{12}]^{2-}$ and its derivatives have attracted the most attention due to its exceptional stability [20]. In addition to $[B_{12}H_{12}]^{2-}$, other experimentally confirmed dianionic boranes ($[B_nH_n]^{2-}$) such as $[B_{10}H_{10}]^{2-}$, $[B_{11}H_{11}]^{2-}$, $[B_9H_9]^{2-}$, $[B_8H_8]^{2-}$, and $[B_7H_7]^{2-}$ [21–24] reveal that these species are stable in their dianionic form. The stability of these clusters can be described by the Wade–Mingos rules [25–28], which indicate that (n + 1) skeletal electron pairs are required for a borane molecule to be stable. Von Ragué Schleyer et al. [7] reported that an increase in the cluster size of borane dianions causes a decrease in the coulomb repulsion and results in a large number of multicenter bonding interaction. Thus, the larger closo-boranes such as $[B_{16}H_{16}]^{2-}$ and $[B_{17}H_{17}]^{2-}$ were found to be more stable than the smaller ones ($n = 5$–11) according to various parameters, such as the vertex basis PRDDO average energies, the synthesis basis cumulative BH addition energy, or disproportionation approach [7].

✉ Fahri Alkan
fahri.alkan@agu.edu.tr

[1] Department of Nanotechnology Engineering, Abdullah Gül University, Kayseri, Turkey

Despite the predicted stabilities of larger closo-boranes, these systems *have not been realized experimentally* as parent borane clusters. The lack of successfully synthesized $[B_nH_n]^{2-}$ clusters for $n > 12$ has been attributed to the exceptional stability of icosahedral $[B_{12}H_{12}]^{2-}$ cluster, which is also referred as *icosahedral barrier* [7]. It should be noted that the icosahedral barrier has been overcome for the cases of carboranes, metallaboranes, and metallacarboranes. The first metal-free 13-vertex carborane has been experimentally realized in 2003 [29]. Since then, a series of 13- and 14-vertex carboranes have been synthesized and structurally characterized [30, 31]. More recently, Zheng et al. have successfully prepared the 15- and 16-vertex carboranes with the introduction of silyl groups to both cage carbons [32]. In the case of metallaboranes and metallacarboranes, several structures beyond the icosahedral barrier have been reported as well [33, 34]. We also note that exploration of new synthetic routes and mechanisms for supraicosahedral systems is still an active research area as several theoretically predicted boron-based polyhedral clusters have not been experimentally synthesized yet.

In addition to supraicosahedral clusters, perfunctionalized clusters can provide new applications and synthetic routes for boron cluster chemistry. Different functional groups have been utilized for this purpose such as halogens, hydroxyl, ester, cyanide, and amine groups [35–42], and electron holding ability of the terminal group is shown to be important to obtain stable clusters for borane derivatives [35, 36]. More recently, selective functionalization of cage B-H bond in polyhedral boranes and carboranes have become a powerful methodology to synthesize a variety of structures with different functional groups [43–46]. On the other hand, the effect of perfunctionalization or selective functionalization on the stability and electronic structure of larger borane clusters ($n \geq 13$) has not been explored. In that aspect, we performed DFT calculations on a series of polyhedral $[B_nX_n]^{2-}$ clusters ($n = 10$, 12, 13, 14, 15, and 16) where X denotes H, F, Cl, Br, CN, BO, OH and NH_2 groups and all the results of larger clusters are particularly given in comparison to $[B_{12}X_{12}]^{2-}$ counterparts, since this cluster has been the central focus of experimental [20, 38, 41, 47] and theoretical [39, 40, 42] investigation among the borane clusters. The effect of substitution on geometries, electronic structure, charge distribution, and formation enthalpies were investigated for these clusters. The results for the borane systems were also compared to selective carborane clusters in the case of formation enthalpies. We hope that our work can provide useful information in terms of cluster stability and possible reaction paths for target systems.

Computational methods

All DFT calculations were carried out using Gaussian 09 [48] package program and Gaussview 5.0 [49] was used for the visualization. Geometries were optimized and electronic structures were investigated for varying sizes of borane clusters and substituted derivatives ($[B_nX_n]^{2-}$, $n = 10$, 12, 13, 14, 15, 16; X = H, F, Cl, CN, BO, OH, and NH_2) using PBE0 functional [50, 51], which was shown to have a good agreement with the experiment in previous work [20]. 6–311++g** basis set was used for the calculations. General structures and point group symmetries of the parent borane dianions are represented in Fig. 1.

Geometry optimizations were followed by the frequency calculation on the same method for the confirmation of the minima on the potential energy surface. As a result of this analysis, there is no negative frequency found which signifies the kinetic stability of the clusters. The vertical and adiabatic detachment energies (VDE and ADE) were determined for the dianions as described in reference 20 with the same level of theory. Benchmark calculations for the electron detachment energies of $[B_{12}X_{12}]^{2-}$ clusters were also performed using different functionals (GGA (BP86 [52, 53]), hybrid (B3LYP [54],PBE0 [50, 51]), and meta-hybrid (M06-2X [55])) to have a clear idea of functional effect on the energies, and the results are provided in the supplementary information (SI). Charge distributions on the clusters were computed using electrostatic potential (ESP)–derived method (charges from electrostatic potentials using a grid (CHELPG [56])) and natural population analysis (NPA [57–60]). Due to the diagonalization problem during NPA for $[B_{12}BO_{12}]^{2-}$ and $[B_{16}(NH_2)_{16}]^{2-}$ with the 6–311++g** basis set, 6-31 g* was used as for these two clusters.

Reaction enthalpies based on –BX addition to $[B_{12}X_{12}]^{2-}$ clusters were calculated and their relation with different substituents is shown in Eq. 1 where $n = 13$, 14, 15, and 16. Moreover, this approach was applied on the transition from 12-vertex to 13- and 14-vertex clusters for singly substituted borane and carborane clusters, as given in Eq. 2 and Eq. 3 ($n = 13$, 14), respectively.

$$\left[B_{12}X_{12}\right]^{2-} + (n-12)B_6X_6H_4 \rightarrow \left[B_nX_n\right]^{2-} + (n-12)B_5X_5H_4 \quad (1)$$

$$\left[B_{12}H_{11}X\right]^{2-} + (n-12)B_6H_{10} \rightarrow \left[B_nH_{n-1}X\right]^{2-} + (n-12)B_5H_9 \quad (2)$$

$$C_2B_{10}H_{11}X + (n-12)B_6H_{10} \rightarrow C_2B_{n-2}H_{n-1}X + (n-12)B_5H_9 \quad (3)$$

For the singly substituted clusters, different isomers were considered for the enthalpy calculations while only the results from lowest-energy isomers were reported.

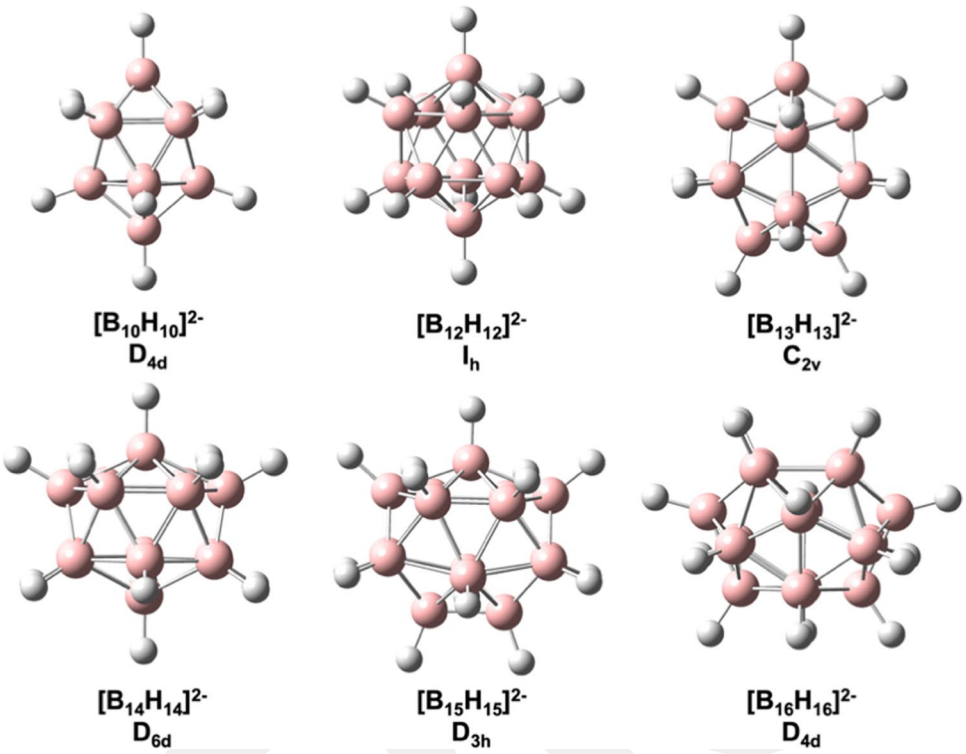

Fig. 1 Structural representation of $[B_{10}H_{10}]^{2-}$, $[B_{12}H_{12}]^{2-}$, $[B_{13}H_{14}]^{2-}$, $[B_{14}H_{14}]^{2-}$, $[B_{15}H_{15}]^{2-}$, and $[B_{16}H_{16}]^{2-}$ clusters along with point group symmetries

These reactions were mainly adapted from the study of Schleyer on the larger boranes [7] and other related studies [61, 62]. The PBE0 results for formation enthalpies were also compared to those obtained with B3LYP [54] and M06-2X [55] for benchmark purposes.

Result and discussions

Geometry

In Fig. 2a, the average bond lengths ($(B\text{-}B)_{avg.}$) between the cage boron atoms are shown with respect to different substituent groups. As shown in the figure, transition from 10- or 12-vertex to larger clusters exhibits a significant increase in $(B\text{-}B)_{avg.}$, and this increase is more pronounced for the lower symmetry 13- and 15-vertex clusters compared to 14- and 16-vertex cases. In case of $[B_{10}X_{10}]^{2-}$ and $[B_{12}X_{12}]^{2-}$, $(B\text{-}B)_{avg.}$ do not show a significant variation for different substituents, whereas there is a noticeable expansion of the cage structure for larger clusters ($n \geq 13$) upon substitution with the halogen atoms. For these clusters, $(B\text{-}B)_{avg.}$ show a maximum increase of 0.017 Å, 0.021 Å, 0.027 Å, and 0.033 Å for 13-, 14-, 15-, and 16-vertex clusters, respectively, with the substitution of X = Br compared to the case where X = H.

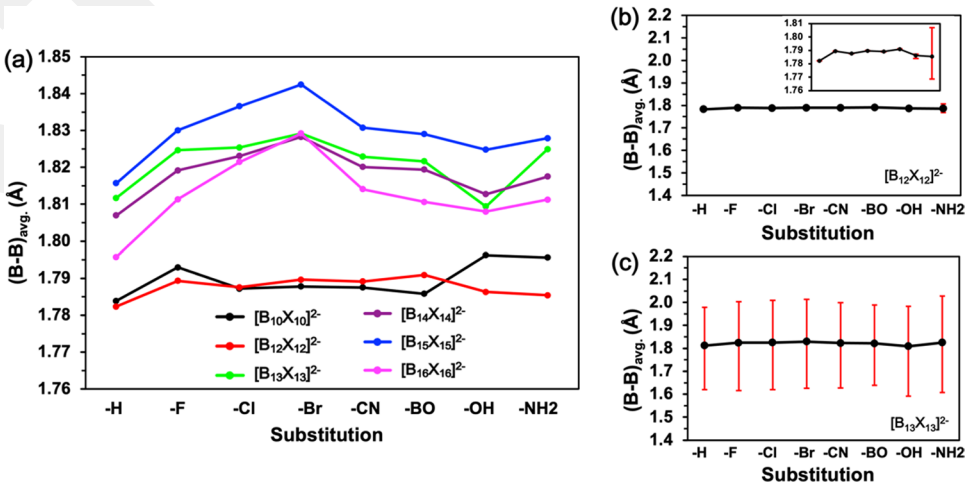

Fig. 2 **a** The average B-B bond lengths or $(B\text{-}B)_{avg.}$ (Å) for cage boron atoms in $[B_nX_n]^{2-}$ clusters, and deviations in the $(B\text{-}B)_{avg.}$ for **b** $[B_{12}X_{12}]^{2-}$ and **c** $[B_{13}X_{13}]^{2-}$ with respect to different substitutions.

In the case of $[B_{12}X_{12}]^{2-}$, clusters exhibit an almost perfect icosahedral (I_h) symmetry for single-atom substitutions (X = F, Cl, and Br) or substitutions with linear geometry (X = CN and BO), whereas the geometries show slight distortions from I_h symmetry with OH and NH_2 substitution. The deviations in $(B\text{-}B)_{avg.}$ are calculated to be 0.002 Å and 0.02 Å for OH and NH_2, respectively, as illustrated in Fig. 2b. In contrast to $[B_{12}X_{12}]^{2-}$, different substitutions generally show similar deviations for the $(B\text{-}B)_{avg.}$ of larger clusters (Figure S1), especially for the cases with lower point group symmetries such as $[B_{13}X_{13}]^{2-}$as illustrated in Fig. 2c. For $[B_{14}X_{14}]^{2-}$ and $[B_{16}X_{16}]^{2-}$, the calculated deviations for the $(B\text{-}B)_{avg}$ show a slight increase with OH and NH_2 substitution similar to the case in $[B_{12}X_{12}]^{2-}$.

Electronic structure

Figure 3a–f shows the pictorial representation of frontier orbitals along with their energies for different substituents of the investigated systems. As seen from the figure, the

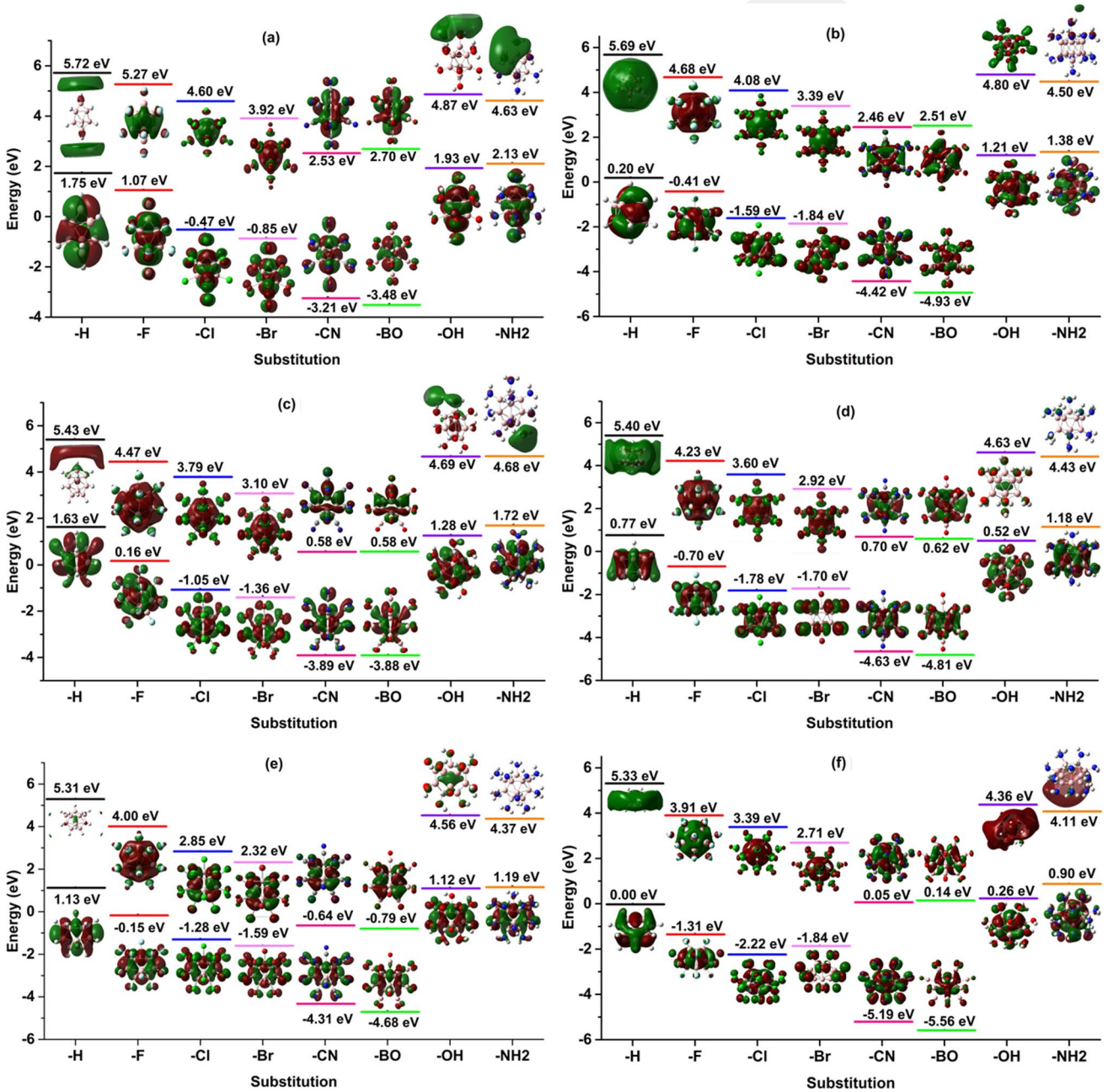

Fig. 3 HOMO–LUMO levels of **a** $[B_{10}X_{10}]^{2-}$, **b** $[B_{12}X_{12}]^{2-}$, **c** $[B_{13}X_{13}]^{2-}$, **d** $[B_{14}X_{14}]^{2-}$, **e** $[B_{15}X_{15}]^{2-}$, and **f** $[B_{16}X_{16}]^{2-}$ clusters calculated with PBE0/6–311++g**

energetics of frontier orbitals show a similar trend for all dianion clusters, except for the case of Br substitution. For halogen substitution, both HOMO and LUMO levels of 10-, 12-, 13-, and 15-vertex clusters exhibit a monotonic stabilization from F to Br as a result of -I (inductive) effects on the boron cage. In the case of $[B_{14}Br_{14}]^{2-}$ and $[B_{16}Br_{16}]^{2-}$ dianions, however, this trend is broken for X = Br, as the HOMO levels of these larger boranes are destabilized with respect to the case in Cl substitution. The population analysis for the HOMO levels reveals that only p orbitals of Br contribute to the HOMO of $[B_{14}Br_{14}]^{2-}$ and $[B_{16}Br_{16}]^{2-}$ clusters, while significant contribution from p orbitals of boron cage appears for the HOMOs in the case of X = Cl or F. The lack of mixing between Br and B orbitals most likely originates from the energy difference (ΔE) parameter between these levels. On the other hand, there is significant mixing predicted between Br and B orbitals for the LUMO level, resulting in the stabilization of this level for $[B_{14}Br_{14}]^{2-}$ and $[B_{16}Br_{16}]^{2-}$ clusters as expected. We note that a similar destabilization in the HOMO level for halogen substitution was reported previously [38] for $[B_{12}X_{12}]^{2-}$clusters as well; however, the monotonic trend was shown to be broken for X = I in this case instead of X = Br found for larger cluster series in this study.

In all cases of clusters regardless of their size or symmetry, the highest stabilization for both HOMO and LUMO levels is seen for the cases of isoelectronic BO and CN substitution, as a result of large -M (mesomeric) effect on the boron cage. Interestingly, this stabilization appears to be higher in amount than that of $[B_{12}X_{12}]^{2-}$ for all the others. In comparison, OH substitution generally exhibits a large destabilization for HOMO and LUMO levels as a result of + M effect. It should be noted that the substituent effects on HOMO and LUMO energies of all clusters largely resemble the mesomeric (± M) and inductive (± I) effects observed in *π-conjugated systems* [63–65] as illustrated in SI (Figure S2) for the 9,10-substitution of anthracene. In that regard, we expect that substitution effects on boron-containing clusters should generally follow the trends that are obtained for a large set of π-conjugated systems in the literature.

For the investigated systems, the positive HOMO energies can be interpreted to indicate unstable charge for the dianion clusters, while this can also be a result of the employed theoretical methodology. For instance, the positive HOMO energy of the $[B_{12}H_{12}]^{2-}$ molecule in the gas phase, which was proven to be stable [20], is shown to be slightly positive with PBE0 functional while the same HOMO energy is determined to be negative with M06-2X functional. It should be noted that the percentage of exact Hartree–Fock (HF) exchange in the level of theory can be significant for such predictions as illustrated for $[B_{12}H_{12}]^{2-}$ in Fig. S3. In comparison, *hypercloso*-$[B_{12}OH_{12}]$ was found to have a positive reduction potential in solution, while it was also reported that the electronic stability decreases upon substitution with the hydroxyl group compared to the case with other functional groups [42]. As for the stability in the gas phase, it is quite clear that $[B_{12}(OH)_{12}]^{2-}$ or $[B_{12}(NH_2)_{12}]^{2-}$ molecules with significantly higher HOMO values, is most likely not electronically stable, which is supported by the negative adiabatic electron detachment energies (ADEs) as well (vide infra). We also note that the energy of the frontier orbitals for the case of OH or NH_2 substitution monotonically decrease with the cluster size for even numbered clusters. In fact, the difference in the energy of HOMO between $[B_{12}H_{12}]^{2-}$ and $[B_{12}OH_{12}]^{2-}$ is predicted to be 1.01 eV whereas the same difference in the case of $[B_{16}X_{16}]^{2-}$ is only 0.26 eV. Interestingly, for $[B_{13}X_{13}]^{2-}$ and $[B_{14}X_{14}]^{2-}$, HOMO even becomes more stable for the case of OH substitution compared to the case where X = H. This is most likely the result of the fact that large + M effects induced by OH or NH_2 groups, which increase the π electron density on the boron cage significantly, can be compensated more easily in the case of larger clusters.

In addition to the electronic structure, both VDEs and ADEs were calculated with different DFT functionals, and the results were given in SI for $[B_{12}X_{12}]^{2-}$ (Table S1 and S2) clusters, respectively. PBE0 functional which was recommended by previous studies [20, 40] as a cost-effective alternative to CCSD(T) method was used as reference method in this study. Note that this functional was shown to yield reliable results for VDEs of H and F substituents, but it underestimates the VDE values for Cl and Br substituted dianions [20, 38]. It should also be mentioned that the BP86 functional with no exact HF exchange highly underestimates the VDEs compared to the case with PBE0, while approximate results were obtained with B3LYP as expected, which has similar HF exchange contribution. On the other hand, M06-2X overestimates the VDEs due to the high ratio of HF exchange in the functional. The VDEs given in Fig. 4 show a quite similar trend for all cluster sizes, except for the Br substituent. Unlike the others, VDE value of $[B_{14}Br_{14}]^{2-}$ and $[B_{16}Br_{16}]^{2-}$ is lower than those of Cl substituted ones. Notice that a similar discrepancy between 14- and 16-vertex clusters and the others has been found for the HOMO levels as well. Both results account for a decrease in the electronic stability in $[B_{14}Br_{14}]^{2-}$ and $[B_{16}Br_{16}]^{2-}$, which is due to the lack of mixing between Br and B p orbitals. Since VDE is a parameter which is directly related to the electronic stability of the molecule, it can be said that the highest stability for $[B_nX_n]^{2-}$ dianions was found for the BO substituent followed by CN substituent, as also stated for $[B_{12}X_{12}]^{2-}$ clusters in previous studies [39, 40]. Figure 4 also shows that the energy required to eject an electron from the dianions is not directly related to the cluster size. VDEs of only $[B_{16}X_{16}]^{2-}$ and some derivatives of $[B_{14}X_{14}]^{2-}$ lie above the icosahedral

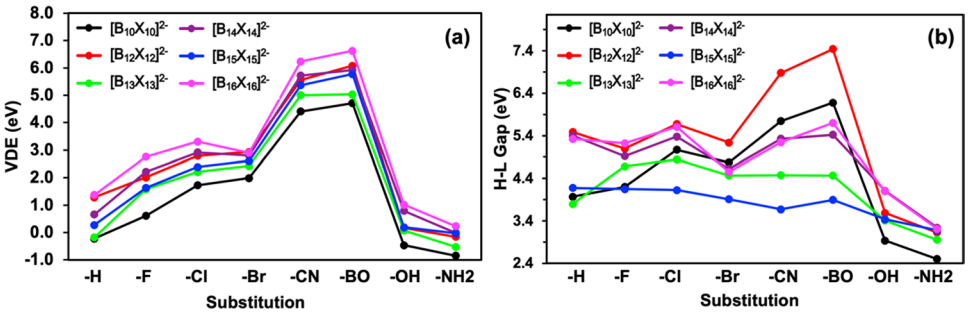

Fig. 4 Comparison of calculated **a** VDE values and **b** H–L gaps for the clusters with different substituents using PBE0/6–311++g** level of theory

boron cluster, which may indicate higher stability for these clusters.

Reaction energies

In addition to the electronic structure analysis, we have performed an investigation for the formation enthalpies ($\Delta H_{add.}$) of larger borane clusters from icosahedral $[B_{12}X_{12}]^{2-}$ with a focus on the effect of substitution on icosahedral barrier. The single step reaction has been adapted from the seminal work of Schleyer et al. [7], which has been employed in following studies investigating borane and carborane clusters [61, 62]. The results for the $[B_nX_n]^{2-}$ are summarized in Table 1 for PBE0/6–311++g** level of theory, whereas the same values are tabulated in Table S3 for B3LYP and M06-2X for comparison. We note that while calculated ΔH_{add} with PBE0 and M06-2X functionals show a good agreement, ΔH_{add} values obtained with B3LYP are somewhat larger, especially for the cases of $n = 15$ and 16. In comparison, all functionals yield similar trends with respect to the substitution effect on the ΔH_{add}.

As shown by Schleyer et al. [7] and later confirmed in other works [61], there is a large gain in stability for the formation of $[B_{12}H_{12}]^{2-}$ cluster with respect to neighboring clusters in size. This is also seen in our investigation as the calculated ΔH_{add} for $[B_{13}H_{13}]^{2-}$ cluster is quite large (42.33 kcal/mol), while ΔH_{add} for the formation of $[B_{12}H_{12}]^{2-}$ from $[B_{10}H_{10}]^{2-}$ is calculated to be − 91.45 kcal/mol. This exceptional stability of $[B_{12}H_{12}]^{2-}$ is often associated with the icosahedral barrier. We note that icosahedral barrier in this context does not refer to an actual energy barrier between two minima and the transition state; however, one should still expect a large energy barrier for the formation of $[B_{13}H_{13}]^{2-}$ from $[B_{12}H_{12}]^{2-}$ as a result of Hammond's postulate. The ΔH_{add} values are also positive for $n = 14$ and 15 cases, whereas it finally becomes negative for the case of $[B_{16}H_{16}]^{2}$, which is also in agreement with the previous work [7]. To understand the effect of substitution more clearly, we illustrated the change in calculated $\Delta H_{add.}$ for each cluster relative to the case where X = H, respectively, in Fig. 5a. For all clusters, it is seen that the energy barrier becomes larger with the halogen substitution with an increasing trend as F → Cl → Br. The larger energy barriers are also obtained for X = CN cases with respect to X = H; however, calculated ΔH_{add} are not as large as the halogen substitution for almost all cases. A further reduction is seen with BO substitution, which shows very similar results with the unsubstituted borane clusters for the calculated ΔH_{add}. These results are most likely related to the increasing -M effect with CN and BO substitution compared to the halogens. In comparison, the most intriguing results are obtained for the energy barriers when *substituents with strong + M effects* are introduced. In the case of OH substitution, $\Delta H_{add.}$ is reduced by ~ 7 kcal/mol compared to the X = H case for $[B_{13}X_{13}]^{2-}$, whereas this reduction further increases to ~ 15 kcal/mol with NH_2 substitution. For larger clusters such as $[B_{15}X_{15}]^{2-}$ and $[B_{16}X_{16}]^{2-}$, however, OH substitution shows an increase in the ΔH_{add}, whereas NH_2 substitution still shows substantial decrease in the calculated ΔH_{add} compared to the case where X = H, which most likely results from stronger + M effects of NH_2 group.

Table 1 Calculated formation enthalpies ($\Delta H_{add.}$)* of $[B_nX_n]^{2-}$ clusters from icosahedral $[B_{12}X_{12}]^{2-}$ with PBE0/6–311++g** level of theory

Clusters	ΔH (kcal/mol)							
	H	F	Cl	Br	CN	BO	OH	NH_2
$[B_{13}X_{13}]^{2-}$	42.33	46.06	53.43	56.12	46.53	40.37	35.10	27.01
$[B_{14}X_{14}]^{2-}$	3.43	17.70	26.92	32.33	13.26	3.35	3.01	− 15.62
$[B_{15}X_{15}]^{2-}$	3.72	31.03	44.12	52.73	20.65	3.87	24.26	− 23.84
$[B_{16}X_{16}]^{2-}$	− 16.02	20.62	39.10	52.00	9.57	− 14.46	22.60	− 41.97

*The $\Delta H_{add.}$ values are calculated based on the addition reaction $[B_{12}X_{12}]^{2-} + (n\text{-}12)\,B_6X_6H_4 \rightarrow [B_nX_n]^{2-} + (n\text{-}12)B_5X_5H_4$ where $n = 13$, 14, 15, and 16

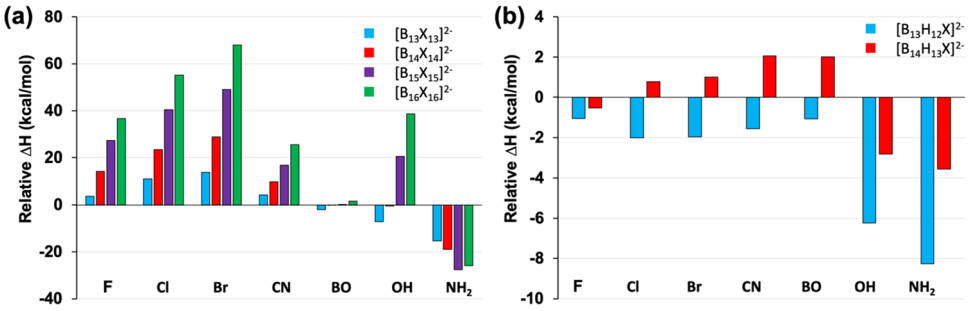

Fig. 5 **a** Calculated relative ΔH_{add} values for the formation of perfunctionalized boron clusters based on the reaction $[B_{12}X_{12}]^{2-} + (n\text{-}12)B_6X_6H_4 \rightarrow [B_nX_n]^{2-} + (n\text{-}12)B_5X_5H_4$ ($n = 13$, 14, 15, and 16) and **b** calculated relative ΔH_{add} values for the formation of single-substituted boron clusters based on the reaction $[B_{12}H_{11}X]^{2-} + (n\text{-}12)B_6H_{10} \rightarrow [B_nH_{n-1}X]^{2-} + (n\text{-}12)B_5H_9$ ($n = 13$ and 14). For all substitution, ΔH_{add} are scaled relative to the case where X = H. All values are obtained with PBE0/ 6–311++g** level of theory

In order to evaluate the effect of single substitution instead of perfunctionalization, ΔH_{add} was also calculated for the formation of 13- and 14-vertex clusters based on the addition reaction (Eq. 2). As shown in Fig. 5b and Table S4, single substitution for the 13-vertex cluster exhibits quite different results for the calculated ΔH_{add} compared to the case of perfunctionalization. For the single substitution of 13-vertex cluster, all functional groups result in lowering the ΔH_{add} values compared to the non-substituted case. This result most likely originates from the reduced symmetries in the case of single-substituted clusters. We note that $[B_{12}H_{12}]^{2-}$ cluster exhibits the *highest symmetry* (I_h point group), whereas $[B_{13}H_{13}]^{2-}$ exhibits the *lowest symmetry* (C_{2v} point group) among the investigated systems (Fig. 1). This is also the case for the perfunctionalized clusters except for OH and NH_2 substitution as discussed previously (Fig. 2). For this reason, the effect of reduced symmetry on the stability of the clusters is expected to be largest for the 12-vertex cluster, while it is expected to be lowest for the 13-vertex cluster. It should also be noted that while there is a reduction in the icosahedral barrier for all single-substituted systems of $[B_{13}H_{12}X]^{2-}$, this reduction is further pronounced for OH and NH_2 substitution due to strong + M effects as expected from the results of perfunctionalized systems. In the case of $[B_{14}H_{13}X]^{2-}$, the effect of reduced symmetry on the stabilities of the parent $[B_{12}H_{12}]^{2-}$ (I_h point group) and $[B_{14}H_{14}]^{2-}$ (D_{6d} point group) clusters are expected to be similar as both clusters are highly symmetric. In this case, icosahedral barrier is *still reduced* with OH and NH_2 substitution as a result of electronic effects, while Cl, Br, CN, and BO substitution shows an increase in the ΔH_{add} values compared to non-substituted clusters.

In addition to borane clusters, we also explored the effect of single substitution on the formation of 13- and 14-vertex carborane clusters in a similar manner as shown in Fig. 6 and Table S5. We note that the icosahedral barrier is also present for carboranes; however, it is calculated to be

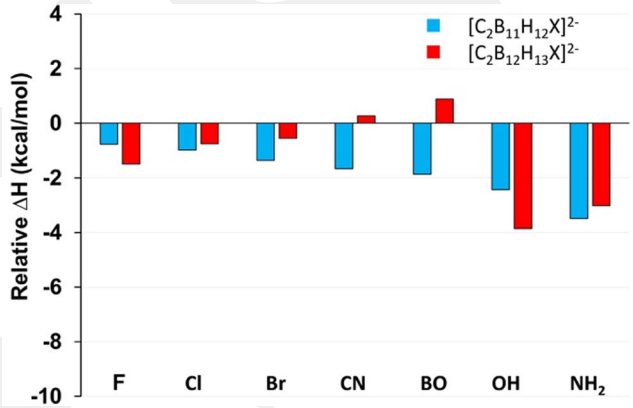

Fig. 6 Calculated relative ΔH_{add} values for the formation of single-substituted carborane clusters based on the reaction $C_2B_{10}H_{11}X + (n\text{-}12)B_6X_6H_4 \rightarrow C_2B_{n-2}H_{n-1}X + (n\text{-}12)B_5X_5H_4$ ($n = 13$, 14). For all substitution, ΔH_{add} are scaled relative to the case where X = H. All values are obtained with PBE0/ 6–311++g** level of theory

substantially lower compared to the case in borane clusters [61]. As shown in Fig. 6, the effect of single substitution on the energetics of icosahedral barrier for carboranes also follows a similar trend compared the case of boranes (Fig. 5b). For carboranes, however, the reduction in the barrier with OH and NH_2 substitution is not as high, which most likely results from the fact that the symmetry is already reduced for the parent $C_2B_{10}H_{12}$ cluster compared to $[B_{12}H_{12}]^{2-}$. In general, our findings indicate that both symmetry and electronic effects can play an important role in reducing the icosahedral barrier for the investigated systems. As mentioned earlier, this barrier mainly originates from exceptional stability of 12-vertex clusters. Through substitution, it can be substantially reduced, especially for the 12-vertex to 13-vertex transition, by *destabilizing the 12-vertex clusters* with functional groups exhibiting *strong + M effects*, and *reducing the symmetry* with bulky ligands.

Population analysis

Charge distribution through the clusters can provide a deeper understanding about where the electron loss is occurred from and how the stabilities are connected to the charge distribution. Therefore, we utilized two methods to obtain the atomic partial charges: NPA and CHELPG. While the NPA charge is derived from the summation over all-natural atomic orbitals (NAOs) of a given atom, the atomic charges are fitted to reproduce the molecular electrostatic potential (MEP) at a number of points around the molecule in the latter method [56, 60]. NPA and CHELPG charges are represented as the summed-up charges for equivalent atoms in the core and surrounding substituent regions in Fig. 7 and Figure S4, respectively.

Although the magnitudes of the charges vary depending on the population analysis method, both give similar results for all clusters except the ones with X = H. Unlike for other derivatives, NPA and CHELPG methods give opposite results for all dianions for this case as the negative partial charges appear on B atoms, and H atoms have positive partial charges with the NPA method, whereas the opposite is true in the case of CHELPG method. This discrepancy has also been previously reported for (car)borane studies [20, 66]. Even though there is still a debate on the reliability of population methods for the calculated H partial charges in (car)boranes, CHELPG method is likely to produce a more accurate description, since the electronegativity difference between B and H, as well as the previous experimental evidence [66–71], suggest more negative H atoms and more positive B atoms for these systems.

For all fluorinated clusters, the boron cage is positively charged while surrounded by the highly negative F substituent shell, and it becomes much more positive with increasing cluster size. Switching to the less electronegative Cl substituent, the shell regions of the clusters are still more negative than the core part, but the differences between two regions are less than the F substitution, and the substituents seem not to have a considerable effect on the charge distribution. With the Br substituent, the charges are more uniformly distributed throughout the smaller dianions and the charge difference between inner and outer shells are small, while boron cage appears to become more negative region unlike the case in X = Cl and X = F, with an increasing strength via increasing cluster size. In the previous work with halogen-substituted $[B_{12}X_{12}]^{2-}$ clusters, Warneke et al. [38] showed that the electron detachment, which is determined by the HOMO position, occurs from the more positively charged region of the molecule. As a result, a decrease in the stability of the clusters for X = I and X = At substituents was shown to originate from the fact that HOMO level mainly originates from the electrons of the substituent with significant reduction in the contribution of the core atoms. This is also the case in stability of $[B_{14}Br_{14}]^{2-}$ and $[B_{16}Br_{16}]^{2-}$ in this study, which was predicted to exhibit a more negative

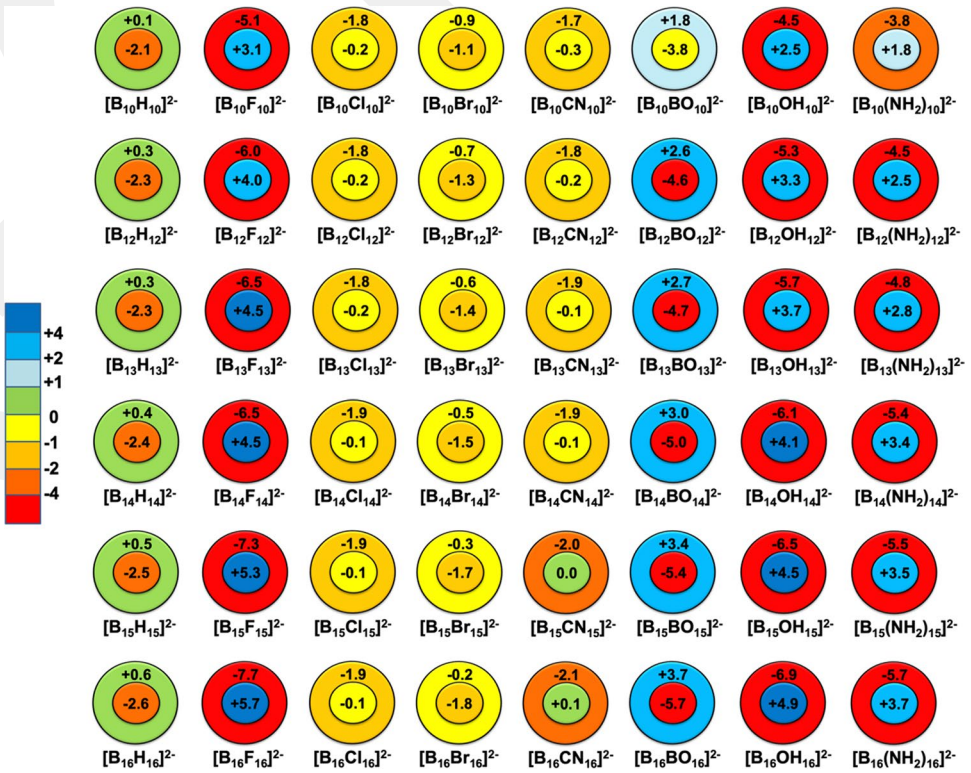

Fig. 7 Schematic representation of the NPA charge distribution in the dianions in terms of an inner core ($B_{10}/B_{12}/B_{13}/B_{14}/B_{15}/B_{16}$) and an outer shell ($X_{10}/X_{12}/X_{13}/X_{14}X_{15}/X_{16}$). The same charge distribution with CHELPG method is illustrated in Figure S4

core compared to the substituent shell. For diatomic substituents, the charge on the boron cage also depends on the electronegativity of the atom which is directly bonded to the cage. For X = CN, the total partial charge on the boron cage in all clusters is quite small, while very positive and very negative charges are predicted for X = OH/NH_2 and X = BO cases, respectively.

Conclusion

In this work, we have performed a benchmark study for the electronic structure and relative stability of $[B_nX_n]^{2-}$ clusters (X = H, F, Cl, Br, CN, BO, OH, NH_2) with respect to substituent effects. In the case of electronic structure, BO and CN substitution showed a large stabilization for the HOMO/LUMO and electron detachment energies as a result of large -M effect while OH and NH_2 substitution resulted in the opposite due to + M effect on the boron cage. For halogen substitution, the inductive effects of the substituents became more dominant than their mesomeric effect and electronic stabilization was provided by -I effect on the boron cage. For all cases, substitution effects on the electronic structure of boron clusters showed a striking resemblance to the ± M and ± I effects observed for the π-conjugated systems.

In addition to the effects on electronic structure, we have examined the substituent effect on the formation enthalpies for larger boron clusters with the addition of BX groups to $[B_{12}X_{12}]^{2-}$. For halogen and CN substitutions, the icosahedral barrier showed an increase compared to X = H case, whereas functionalization with substituents with + M effect such as OH and NH_2 showed a considerable reduction the icosahedral barrier. Similar results were also found for selective carborane clusters. In general, our results showed that the icosahedral barrier can be reduced through substitution by destabilizing the $[B_{12}X_{12}]^{2-}$ cluster with symmetry-reducing ligands or ligands with + M effects rather than stabilizing the larger clusters. To the best of our knowledge, benchmarking the functionalized closo-borane dianions through their electronic structures and stability relations on the basis of formation reactions have not been discussed previously. In that regard, we hope that this study can be a useful guide for future experimental and theoretical investigations for such systems.

Supplementary Information The online version contains supplementary material available at https://doi.org/10.1007/s00894-021-04980-1.

Acknowledgements We would like to thank Prof. Hakan Usta for carefully reading the manuscript and their valuable recommendations. We are indebted to Abdullah Gül University for making the facilities of the High-Performance Computing (HPC) center available for our computational work.

Author contribution DT, FA, and MD conceived the idea and planned the computations in this study. DT ran the most of the computations and wrote the first draft for this manuscript. FA supervised the project. MD edited and reviewed the manuscript prior to submission. All authors approved the contents of this manuscript.

Funding This work was supported by Research Fund of Abdullah Gül University (Project Number: FDK-2018–122).

Availability of data and material All relevant data are available in the electronic supplementary information.

Code availability Gaussian 09 Revision A.02 is used for all the calculations in this work. Gaussview 5.0 is used for the visualization and generation of figures in the article.

Declarations

Ethics approval Not applicable.

Conflicts of interest The authors declare no competing interests.

References

1. Gonzalez Szwacki N, Sadrzadeh A, Yakobson BI (2007) B80 fullerene: an ab initio prediction of geometry, stability, and electronic structure. Phys Rev Lett 98(16):166804
2. Cheng L (2012) B14: an all-boron fullerene. J Chem Phys 136(10):104301
3. Shen YF, Xu C, Cheng LJ (2017) Deciphering chemical bonding in BnHn2- (n = 2–17): flexible multicenter bonding. RSC Adv 7:36755–36764
4. Lipscomb WN, Epstein IR (1971) Boron hydride valence structures. Topological approach. Inorg Chem 10(9):1921–1928
5. Bicerano J, Marynick DS, Lipscomb WN (1978) Molecular orbital studies on large closo boron hydrides. Inorg Chem 17(12):3443–3453
6. Williams RE (1992) The polyborane, carborane, carbocation continuum: architectural patterns. Chem Rev 92(2):177–207
7. Schleyer PR, Najafian K, Mebel AM (1998) The large closoborane dianions, B(n)H(n)(2-) (n = 13–17) are aromatic, why are they unknown? Inorg Chem 37(26):6765–6772
8. Brown LD, Lipscomb WN (1977) Closo boron hydrides with 13 to 24 boron atoms. Inorg Chem 16(12):2989–2996
9. Grimes RN (2004) Boron Clusters Come of Age. J Chem Educ 81(5)
10. Byun D et al (1994) Photoemission from gaseous and condensed molecular carborane cluster molecules. J Electron Spectrosc Relat Phenom 69(2):111–116
11. Fang H, Jena P (2019) Stable tetra- and penta-anions in the gas phase. Angew Chem Int Ed Engl 58(33):11248–11252
12. Joshi M, Ghanty TK (2019) Lanthanide and actinide doped B12H12(2-) and Al12H12(2-) clusters: new magnetic superatoms with f-block elements. Phys Chem Chem Phys 21(42):23720–23732
13. Lee S et al (1992) Structures of selected boranes and carboranes. J Vac Sci Technol A 10(4):881–885
14. Pathak B et al (2011) Borane derivatives: a new class of super- and hyperhalogens. ChemPhysChem 12(13):2423–2428
15. Zahradnik R, Balaji V, Michl J (1991) An SCF study of 10-vertex and 12-vertex boranes and heteroboranes. J Comput Chem 12(9):1147–1156

16. Giri S, Behera S, Jena P (2014) Superhalogens as building blocks of halogen-free electrolytes in lithium-ion batteries. Angew Chem Int Ed 53(50):13916–13919
17. Tutusaus O et al (2015) An efficient halogen-free electrolyte for use in rechargeable magnesium batteries. Angew Chem Int Ed Engl 54(27):7900–7904
18. Zhong M et al (2017) Role of ligands in the stability of BnXn and CBn-1Xn (n = 5–10; X = H, F, CN) and their potential as building blocks of electrolytes in lithium ion batteries. Phys Chem Chem Phys 19(27):17937–17943
19. Maderna A, Knobler CB, Hawthorne MF (2001) Twelvefold functionalization of an icosahedral surface by total esterification of [B12(OH)12]2-: 12(12)-closomers. Angew Chem Int Ed Engl 40(16):2947
20 Apra E et al (2019) A benchmark photoelectron spectroscopic and theoretical study of the electronic stability of [B12H12](2). J Chem Phys 150(16):164306
21. Lipscomb WN, Pitochelli AR, Hawthorne FM (1959) PROBABLE STRUCTURE OF THE B10H10-2 ION. J Am Chem Soc 81(21):5833–5834
22. Kaczmarczyk A, Dobrott RD, Lipscomb WN (1962) REACTIONS OF B10H10-2 ION. Proc Natl Acad Sci U S A 48(5):729–733
23 Klanberg F, Muetterties EL (1966) Chemistry of Boranes. XXVII. New polyhedral borane anions, B9H92- and B11H112-. Inorg Chem 5(11):1955–1060
24 Klanberg F et al (1967) Chemistry of boranes. XXVIII. New polyhedral borane anions, B8H82-, B8H8.-, and B7H72-. Inorg Chem 6(7):1271–1281
25. Wade K (1971) The structural significance of the number of skeletal bonding electron-pairs in Carboranes, the higher boranes and borane anions, and various transition-metal carbonyl cluster compounds. J Chem Soc D 15:792–793
26. Wade K (1976) Structural and bonding patterns in cluster chemistry. Adv Inorganic Chem Radiochem 18:1–66
27. Mingos DMP (1984) Polyhedral Skeletal Electron Pair Approach. Acc Chem Res 17(9):311–319
28. Chen G et al (2019) Rational design of stable dianions and the concept of super-chalcogens. J Phys Chem A 123(27):5753–5761
29. Burke A et al (2003) Beyond the icosahedron: the first 13-vertex carborane. Angew Chem Int Ed Engl 42(2):225–228
30. Zhang J, Xie Z (2014) Synthesis, structure, and reactivity of 13- and 14-vertex carboranes. Acc Chem Res 47(5):1623–1633
31. Deng L, Chan HS, Xie Z (2006) Synthesis, structure, and reactivity of 13-vertex carboranes and 14-vertex metallacarboranes. J Am Chem Soc 128(15):5219–5230
32. Zheng F et al (2020) Synthesis and X-ray characterization of 15- and 16-vertex closo-carboranes. Nat Commun 11(1):5943
33. Deng L et al (2006) Synthesis and structure of 14- and 15-vertex ruthenacarboranes. Angew Chem Int Ed Engl 45(26):4309–4313
34. Deng L, Xie Z (2007) A Journey from 12-vertex to 14-vertex carboranes and to 15-vertex metallacarboranes. Organometallics 26:1832–1845
35. Dreuw A, Zint N, Cederbaum LS (2002) Dianionic tetraborates do exist as stable entities. J Am Chem Soc 124(36):10903–10910
36. Zint N, Dreuw A, Cederbaum LS (2002) Gas-phase stability of derivatives of the closo-hexaborate dianion B6H62-. J Am Chem Soc 124(17):4910–4917
37. Boyd LA et al (2004) Exo-pi-bonding to an ortho-carborane hypercarbon atom: systematic icosahedral cage distortions reflected in the structures of the fluoro-, hydroxy- and amino-carboranes, 1-X-2-Ph-1,2–C2B10H10 (X=F, OH or NH2) and related anions. Dalton Trans 17:2786–2799
38. Warneke J et al (2017) Electronic structure and stability of [B12X12](2-) (X = F-At): a combined photoelectron spectroscopic and theoretical study. J Am Chem Soc 139(41):14749–14756
39. Zhao HM, Zhou J, Jena P (2016) Stability of B-12(CN)(12)(2-): Implications for lithium and magnesium ion batteries. Angew Chem Int Ed 55(11):3704–3708
40. Moon J, Baek H, Kim J (2018) Unusually high stability of B12(BO)122− achieved by boronyl ligand manipulation: theoretical investigation. Chem Phys Lett 698:72–76
41. Boere RT et al (2014) On the oxidation of the three-dimensional aromatics [B(12)X(12)](2-) (X=F, Cl, Br, I). Chemistry 20(15):4447–4459
42. Lee TB, McKee ML (2012) Redox energetics of hypercloso boron hydrides B(n)H(n) (n = 6–13) and B12X12 (X = F, Cl, OH, and CH3). Inorg Chem 51(7):4205–4214
43. Teixidor F, Vinas C (2018) Halogenated icosahedral carboranes: a platform for remarkable applications, in Handbook of Boron Science: With Applications in Organometallics, Catalysis, Materials and Medicine, N.S. Hosmane and R. Eagling, Editors. World Scientific
44. Axtell JC et al (2018) Synthesis and applications of perfunctionalized boron clusters. Inorg Chem 57(5):2333–2350
45. Grimes RN (2016) Carboranes. Academic Press, p 1058
46. Nunez R et al (2016) Electrochemistry and photoluminescence of icosahedral carboranes, boranes, metallacarboranes, and their derivatives. Chem Rev 116(23):14307–14378
47. Avelar A, Tham FS, Reed CA (2009) Superacidity of boron acids H2(B12X12) (X = Cl, Br). Angew Chem Int Ed Engl 48(19):3491–3493
48. Frisch MJ et al (2009) Gaussian 09. Gaussian Inc, Wallingford CT
49. Dennington RD, Keith TA, Milliam JM (2009) GaussView 5.0. Semichem Inc., Wallingford CT
50. Perdew JP, Ernzerhof M, Burke K (1996) Rationale for mixing exact exchange with density functional approximations. J Chem Phys 105(22):9982–9985
51. Adamo C, Barone V (1999) Toward reliable density functional methods without adjustable parameters: The PBE0 model. J Chem Phys 110(13):6158–6170
52. Perdew JP (1986) Density-functional approximation for the correlation energy of the inhomogeneous electron gas. Phys Rev B Condens Matter 33(12):8822–8824
53. Becke AD (1988) Density-functional exchange-energy approximation with correct asymptotic behavior. Phys Rev A Gen Phys 38(6):3098–3100
54. Becke AD (1993) Density-functional thermochemistry. 3. The role of exact exchange. J Chem Phys 98(7):5648–5652
55. Zhao Y, Truhlar DG (2008) The M06 suite of density functionals for main group thermochemistry, thermochemical kinetics, noncovalent interactions, excited states, and transition elements: two new functionals and systematic testing of four M06-class functionals and 12 other functionals. Theoret Chem Acc 120(1–3):215–241
56. Breneman CM, Wiberg KB (1990) Determining atom-centered monopoles from molecular electrostatic potentials - the need for high sampling density in formamide conformational-analysis. J Comput Chem 11(3):361–373
57. Foster JP, Weinhold F (1980) Natural Hybrid Orbitals. J Am Chem Soc 102(24):7211–7218
58. Reed AE, Weinhold F (1983) Natural Bond Orbital Analysis of near-Hartree-Fock Water Dimer. J Chem Phys 78(6):4066–4073
59. Reed AE, Weinhold F (1985) Natural Localized Molecular-Orbitals. J Chem Phys 83(4):1736–1740
60. Reed AE, Weinstock RB, Weinhold F (1985) Natural-Population Analysis. J Chem Phys 83(2):735–746
61. Zhang JJ, Lin ZY, Xie ZW (2015) DFT Studies on structures, stabilities, and electron affinities of closo-supercarboranes C2Bn-2Hn (n=13-20). Organometallics 34(23):5576–5588

62. Liao RB et al (2015) A topological pattern for understanding the structures of boranes and borane analog compounds. Struct Chem 26(1):353–364
63. Krygowski TM, Stepien BT (2005) Sigma- and pi-electron delocalization: focus on substituent effects. Chem Rev 105(10):3482–3512
64. Krygowski TM et al (2014) Aromaticity from the viewpoint of molecular geometry: application to planar systems. Chem Rev 114(12):6383–6422
65 Milian Medina B et al (2007) Effect of fluorination on the electronic structure and optical excitations of pi-conjugated molecules. J Chem Phys 126(11):111101
66. Fanfrlik J et al (2006) Interaction of carboranes with biomolecules: formation of dihydrogen bonds. ChemPhysChem 7(5):1100–1105
67. Klooster WT et al (1999) Study of the N−H···H−B dihydrogen bond including the crystal structure of BH3NH3 by neutron diffraction. J Am Chem Soc 121(27):6337–6343
68. Li J, Zhao F, Jing F (2002) B-Hδ−σ bond as dihydrogen bond acceptor: some theoretical observations and predictions. J Chem Phys 116(1):25–32
69 Lyssebko KA, Antipin MY (2004) Nature of weak inter- and intramolecular interactions in crystals. 1. The F...O and F...H contacts in the crystal of 2-trifluoroacetyl-5-trifluoromethylpyrrole. Russian Chem Bull 53:10–17
70 Planas JG et al (2005) Self-assembly of mercaptane-metallacarborane complexes by an unconventional cooperative effect: a C-H…S-H…H-B hydrogen/dihydrogen bond interaction. J Am Chem Soc 127(45):15976–82
71. Shubina ES et al (1998) Problems of unusual hydrogen bonds between proton donors and transition metal hydrides and borohydrides. Russ Chem Bull 47:817–822